Martian cold spot regions and associated properties during a global dust storm year using MRO/MCS DDR observations

Dissertation submitted in partial fulfilment of the

requirements for the degree of

Master of Science

In

Atmospheric Sciences

By

Nirvan Abhilash

(Roll Number: 420AS2126)

Based on research carried out under the supervision of

Prof. Jagabandhu Panda

Department of Earth and Atmospheric sciences
National Institute of Technology Rourkela
ROURKELA-769008, ODISHA, INDIA

Department of Earth and Atmospheric sciences
National Institute of Technology Rourkela

CERTIFICATE

This is to certify that the dissertation entitled "**Martian cold spot regions and associated properties during a global dust storm year using MRO/MCS DDR observations**" being submitted by **Nirvan Abhilash** (420AS216), in partial fulfilment of the requirements for the degree of **Master of Science** in **Atmospheric Sciences** at National Institute of Technology, Rourkela is an authentic work carried out under my supervision and guidance. To the best of my knowledge, the matter embodied in the Dissertation has not been submitted to any other university/Institute for the award of any degree or diploma.

Prof. Jagabandhu Panda
Dept. of Earth and Atmospheric Sciences
National Institute of Technology, Rourkela
Rourkela-76900, Odisha

Declaration of Originality

Thereby declare that this dissertation entitled "***Martian cold spot regions and associated properties during a global dust storm year using MRO/MCS DDR observations***" represents my original work and effort to the best of my knowledge, it contains no material; previously published or written by another person, nor any material presented for the award of any degree or diploma of National Institute of Technology Rourkela, or any other institution. Works of authors cited in this dissertation have been duly acknowledged under the section "Reference". I am fully aware that in case of any non-compliance detected in future, the Senate of National Institute of Technology Rourkela may withdraw the degree awarded to me on the basis of the present dissertation.

Nirvan Abhilash (Roll No. - 420AS2126)
Dept. of Earth and Atmospheric Sciences
National Institute of Technology Rourkela
May, 2022

ACKNOWLEDGEMENTS

I take this opportunity to express my sincere thanks and deepest sense of gratitude to Prof. Jagabandhu Panda (Head of the Department), Department of Earth and Atmospheric Science, NIT Rourkela for supervising me throughout the tenure of the Dissertation. The Dissertation would have never been completed without his able guidance, constant vigil, careful supervision and inspiration at all stages of the work.

I would also like to show my indebt gratitude to Dr. Bijay Kumar Guha for his scientific inputs regarding the analysis in the Dissertation work. I would also like to thank the scientist of NASA and ESA for providing the Level-2 DDR datasets via PDS MCS/MRO. I would also like to thanks researcher Forget, Millour and ESA for MCD reanalysis data sets.

I would like to express my gratitude to my MAS lab mates, especially Anirban Mandal, Ankan Sarkar and Debashish Paul. for all kinds of technical, scientific and mental support during the tenure for the dissertation work.

I would like to thank my friends and family members for the encouragement and support they provided throughout the work. This Dissertation would not have been possible without them.

Nirvan Abhilash
Roll No. - 420AS2126
NIT Rourkela

ABSTRACT

In the 1970s, Viking and Mariner probes observed the region, where brightness temperatures (nearly surface temperatures) were lesser than 140-148 K. The region of interest was termed cold spots. This work includes the origin of cold spots, associated literature, their spatial and temporal variation etc. The cold spots during the Martian years 33 and 34, were mainly focused to highlight their variability during a global dust storm year in comparison to a year not having a global dust storm. For this purpose, the variability in spatial and temporal manner is emphasized, including seasonal (areocentric longitude), local solar time, altitude wise, along the latitudes, and also for topographic, and non-topographic types. MCS/MRO DDR datasets are used for this purpose. The parameters considered for the analysis include, surface temperature, vertical temperature profile, dust column optical depth, and ice column optical depth, etc. Understanding cold spots and their behavior will help to have an in-depth knowledge regarding the carbon cycle on Mars.

Keywords: - cold spots, dust storms, surface temperature, brightness temperature, column optical density

CONTENTS

LIST OF FIGURES

LIST OF TABLES

1. Introduction

Mars is one of the nearest and most Earth-like planets in our solar system. The discussion on Mars is currently most common in the news and an important topic in the research communities and space agencies worldwide. Like Earth, Mars has polar ice caps. It has an active sub-polar atmosphere that is thermally and topographically driven. Sometimes thermal maxima reach near subpolar latitude due to the eccentricity of Mars and the absence of thermal sink-like ocean bodies (Haberle et al., 1982). It has ice sheets that are believed to preserve millions of years of historical records. There are few but impactful studies and publications on the mars subpolar region through Viking Orbiter, Mars Global Surveyor, Mars Express, Mars Reconnaissance Orbiter etc. There is also the Mars Climate Database containing meteorological fields derived from the GCM model. Thus the mars polar region is a potential storehouse of knowledge unequaled anywhere on Mars (Lorenz et al., 2000). Viking and Mariner probes during the 1970s observed regions of low temperature categorized by Tb < 140-148 K while in some papers it is lesser than 135 K. These temperature ranges are equal to the expected kinetic temperature below CO_2 ice sublimation (Kieffer et al., 1976). Each year seasonal caps of Mars cycle a quarter of the Martian atmosphere (Tillman et al., 1993; Kelly et al., 2006). Thus emphasizing the role of the CO_2 cycle in Martian climate dynamics. Cold spot formation is an essential part of the CO_2 cycle. It can hint at the presence of optically tropospheric thick clouds at an altitude of 30-40 km. Studies using data from Viking Infrared Thermal Mapper (IRTM) (Forget et al., 1995), Mars Global Surveyor (MGS) Thermal Emission Spectrometer (TES) (Titus et al., 2001; Hansen, 1997), and Mars Orbiter Laser Altimeter (MOLA) data (Ivanov et al., 2001 ; Muhleman et al, 2001) suggested that these cold spots were most likely a combination of CO_2 atmospheric condensates and freshly fallen CO_2 snow. There are prominent studies related to cold spots done by Cornwall1 and Titus (2009) on 2001 dust storm cold pots by taking MGS-TES (Mars Global Surveyor -Thermal Emission Spectrometer) data and also by Hayne and Paige (2008) by considering MCS-MRO data. The primary studies relating to cold spots are summarized in the following table (Table 1).

Table 1: Primary literature available on cold spots

Authors	**Remarks**
Cornwall and Titus (2009)	The study mainly emphasized on the spatial and temporal distributions of Martian north polar (and south pole) cold spots

	before, during, and after the global dust storm of 2001. It focused on the differences between topographic and non-topographic cold spots involving half-life, amplitude, and size. In addition, the changes in cold spot behavior were studied during the global dust storm of MY 25 with its conjugate years. The dust storm also seems to have affected the processes of formation, temporal and spatial distribution of cold spots. It tries to provide observational constraints for Mars GCMs and mesoscale models.
Hayne and Paige (2008)	The study focused on the Mars polar cold spots observed through MRO/MCS. The statistical analysis gives that the brightness temperature of polar cold spots from nadir observation correlates (inversely) with the presence of polar clouds viewed at the limb. Taking the radiative transfer model provides insight into the origin of cold spot regions and their role in the polar nighttime. Tropospheric CO_2 polar clouds may persist throughout the polar night, precipitating dry ice and releasing latent heat that adds to the polar thermal balance. It also stated that dust plays a significant role in the origin and evolution of CO_2 polar clouds and their associated cold spot regions.
Cornwall and Titus (2010)	This study focused on the differences of cold spot behavior and characteristics between the north and south polar rings as well as outside the polar rings for both hemispheres. Temporal and spatial changes in southern cold spot behavior prior to and after the global dust storm were also studied. In the north polar ring, cold spot activity is much greater than in the south polar ring. Spots in the south polar ring cold spots often lasted longer and were smaller than the cold spots in the north polar ring. Outside the polar ring, cold spot activity in the south was greater than

	in the north. Cold spots outside the polar ring in the north often formed in association with topographic or terrain features.
Weiss and Ingersoll (2000)	In the paper it tells the possibility that the depletion of CO_2 in the air at the surface the leads to lower CO_2 condensation temperature. Estimated the rate that leads low-molecular-weight air that would disperse into the high-molecular-weight air above and which is generally faster than the rate of supply. This dispersal is stopped if there is a strong temperature inversion (warm air above colder air) near the surface. Which leads to stability issue.

1.1 Theories on the origin of cold spots

Since the discovery of cold spots during the Viking era within the polar region the duration of the polar night has remained an enigma in the scientific community. There are three primary explanations are in discussion in the scientific community.

- Depletion of CO_2 in the atmosphere: Condensation of atmospheric carbon dioxide during polar nights could lead to enrichment of non-condensable phases. Lowering partial pressure of CO_2 leads to a lowering of equilibrium surface temperature (Kieffer et al., 1977).

- CO_2 frost with low emissivity: Non-unit emissivity of surface CO_2 is the due formation of freshly condensed CO_2 ice or frost that leads to low surface emissivity (Ditteon et al., 1977; Kieffer et al., 1979).

- Polar clouds: Optically thick CO_2 and water ice clouds in middle to the high-tropospheric regions could result in lower measured brightness temperatures or surface temperature due to scattering or due to low blackbody temperature emission (Hunt et al., 1980).

The first hypothesis has been ruled out by the scientific community due to the stability constraints and it is feasible only under special circumstances because of dynamic instability (Hess et al., 1979). That leaves us with the second and third hypotheses. Surface temperature below the CO_2 frost point will provide us with a general idea of the location of CO_2 frost supporting the first hypothesis. While vertical temperature point less than CO_2 frost point line with correlation with ice vertical column optical density distribution will provide a general idea on the presence of ice nucleation sites below CO_2 frost point which lead to the formation of CO_2 clouds, supporting the second hypothesis (Neumann et al., 2003; McCleese et al., 2008).

1.2 Topographic and Non-Topographic Cold spots.

Topographic Cold spots are terrain-induced cold spots. It is common near craters, large sudden slope peaks, canyons, and deep valleys. Here air parcel is orographically forced lifted along the surface which causes adiabatic expansion and cooling air parcel (Forget et al., 1998) or gravity waves leading to condensation (Colaprete et al., 2002; Toon, 2002; Tobie et al., 2003). They related spatially with surface features. Non-Topographic Cold spots are independent of surface features that are formed due to the manifestation of clouds or snow (Forget et al., 1998).

1.3 Objectives of the Study and organization

Based on the interests, available literature, data availability and feasibility, the following objectives are decided for the dissertation works:

- Finding cold spot regions through MCS DDR data sets
- Analyzing cold spot regions property, viz., its spatial and temporal variation
- How MY 34 dust storm has impact on cold spot regions' properties
- Correlating dust particle, water ice, CO_2 frost points and cold spot region formation

For fulfilling the defined objectives of the study, MCS observations from MRO were considered. The following section describes about the data used and methodology adopted. The results are discussed in section 3, and conclusions drawn from the study are highlighted in the last section of this report.

2. Data and Methodology

2.1. MRO-MCS

Mars Reconnaissance Orbiter (MRO) is a probe placed in a sun-synchronous polar orbit around Mars in the year 2006. As compared to other space crafts sent to Mars it has collected the most amount of information. It continuously sends information from 2006 to the present (2022). It has the Mars Climate Sounder (MCS) instrument in it. This optical telescope takes both limb and nadir observation through the Martian atmosphere. It provides data on basic Martian weather variables like pressure, temperature, humidity, and dust density. MCS is a nine-channel infrared radiometer, which consists of one visible/near-infrared (0.3 μm to 3.0 μm) and eight far-infrared (12 μm to 50 μm) channels (Table 2). MCS takes a vertical profile of weather variables by staking 21 samples simultaneously with the measurements centered nearly 5 km apart at the limb.

Table 2: Channels in Mars Climate Sounder radiometer

Channels	Bandpass cm^{-1}	Band Center -μm	Measurement Functions
A1	595-615	16.5	Temperature 20-40 km
A2	615-645	15.9	Temperature 40-80 km, Pressure
A3	635-665	15.4	Temperature 40-80 km, Pressure
A4	820-870	11.8	Dust and Condensate (D&C) extinction 0-80 km.
A5	400-500	22.2	Temperature 0-20 km, D&C extinction 0-80 km.
A6	3300-33000	1.65	Polar Radiative Balance.
B1	290-340	31.7	Temperature 0-20 km, D&C extinction 0-80 km.
B2	220-260	41.7	Water vapor 0-40 km, D&C extinction 0-80 km.
B3	230-245	42.1	Water vapor 0-40 km, D&C extinction 0-80 km.

2.2. Data Levels

Data generated by MCS is stored, modified, and updated into levels. These documents use both NASA-level systems and the Committee on Data Management and Computation (CODMAC) data level numbering system to describe the Processing Levels. The data level is further described in Table 3. These data sets are available at (https://pds-atmospheres.nmsu.edu/) .

Table 3: Data Level chart used in PDS.

NASA	COMAC	Description
Packet data	Raw Level 1	Contains telemetry data streams as received at the ground

		stations, with science and engineering data embedded.
Level-0	Edited -Level 2	These types of datasets are not calibrated count values and do not have any physical quantities, and is raw telemetry production. Instrument science data (e.g. counts, raw voltage) at full resolution, time-ordered with duplicates and transmission errors removed. The dataset's meta-data, such as observation time and exposure time, are contained by the ancillary data. The ancillary data is produced using ranging data as well as the raw telemetry data. However, these datasets are not produced as they are scientifically irrelevant.
Level 1A	Calibrated -Level 3	Similar to the L0 data, it also contains raw data which has no physical quantity. Data have been located in space and may have been transformed (e.g., calibrated, rearranged) in a reversible manner and packaged with needed ancillary and auxiliary data (e.g., radiances with the calibration equations applied).
Level 1B	Calibrated -Level 4	Irreversibly transformed data (e.g., resampled, remapped, calibrated) values of the instrument measurements (e.g., magnetic field strength, radiances data).
Level 2	Derived - Level 5	Geophysical parameters data, derived from Level 1 data, and located in spatial and temporal commensurate with instrument location, pointing, and sampling.
Level 3	Derived - Level 5	Geophysical parameters data mapped onto uniform space-time grids.

2.3 DDR (Derived Data Records)

The DDR (Derived Data Records) are generated by the MCS instrument team, JPL. These products are derived from Reduced Data Products (RDR) of MRO-MCS data sets. DDR datasets are categorized to put in the group of NASA Level 2 data. It contains the profile of successfully estimated retrieval, retrieved geophysical parameters, observation errors, and profiles in space and time located by the geometry information property. Each DDR file is arranged in 4-hour intervals for each sol day. Further information on MCS/DDR data is given at (https://atmos.nmsu.edu/PDS/data/MROM_1173/DOCUMENT/DP_SIS.PDF).

2.4 Working of Codes

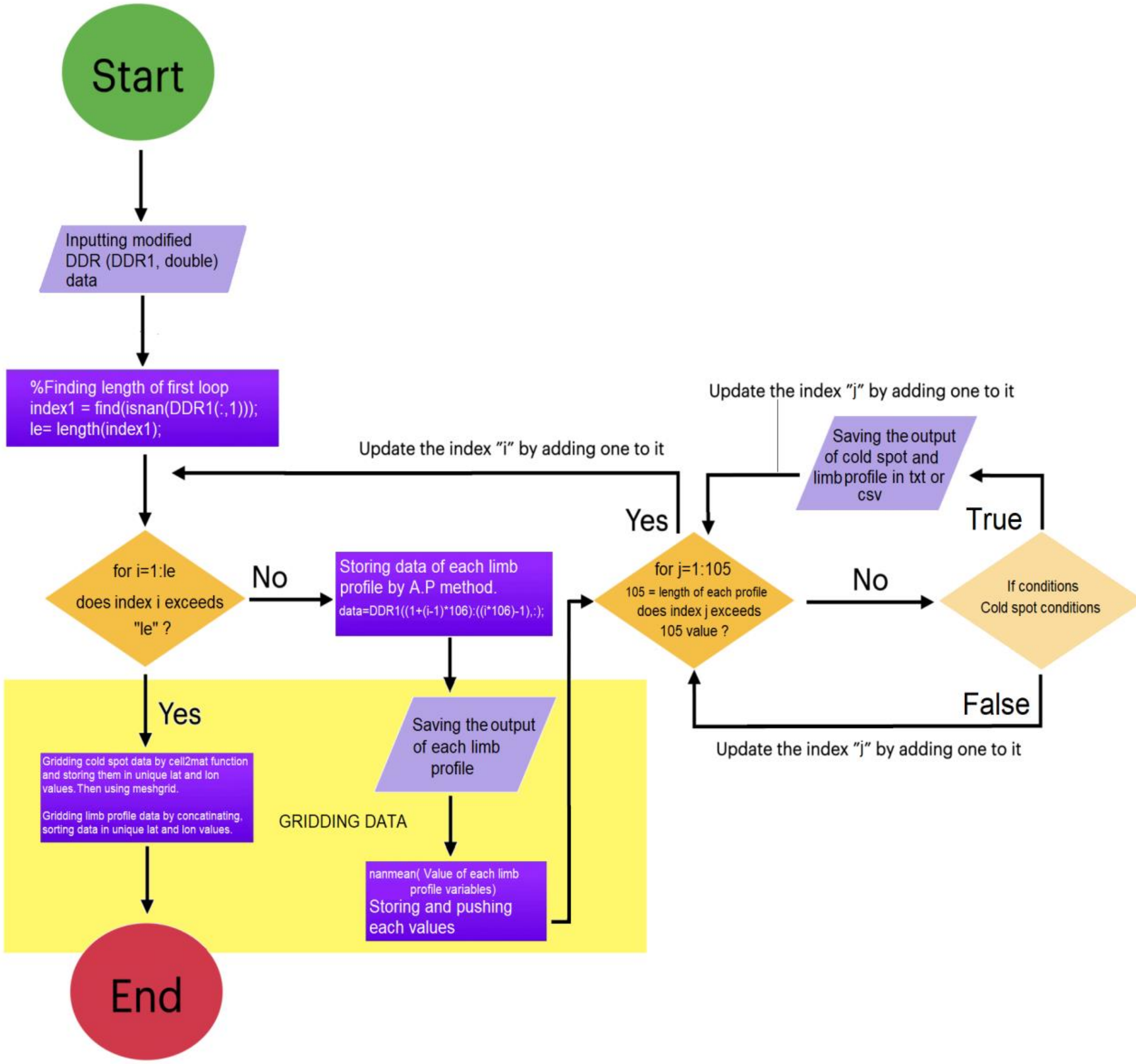

Figure 1. The flow chart on reading, gridding, and extracting limb profile and cold spots data from DDR.TAB file.

The DDR data is in .TAB files. This means .TAB files contain tab-separated values. In MATLAB, used detect Import Options (opts) to read DDR.TAB files and also used dir namelist with a loop to read all targeted files. Extracting cold spots region data from DDR data files. First getting DDR modified files named "DDR1" containing readable double data of all specified concatenated files and passing through two loops. The first loop extracts each limb profile data in a DDR1 data separated by the first column “NaN” header. Inside the first loop, arithmetic progression method (A.P method) has been used to extract each limb's data

data=DDR1((1+(i-1)*106):((i*106)-1),:) **(code 1)**

Then inside the first loop, there is a second loop that runs up to the length each limb profile that is 105. Inside the second loop, there is an if conditional statement. This conditional statement is used to find cold spot data points in the profile.

if(Vertical profile temp<= CO_2 frost line & Vertical height<=40.0000 km & Vertical height>=5.0000 km & Surface temp<140.00 K) **(code 2)**

After satisfying this condition the data is extracted and then the data is arranged, common values are averaged and gridded. These gridded values are helpful for spatial plots. Hence somewhat converting Level 2 data to Level 3 data. Topographic and Non-topographic cold spot regions are found by superimposing spatial retrieved cold spot data from DDR data sets onto the MOLA map in the JMARS tool. Codes are provided at (https://github.com/NirvanAbhilash/MCS_DDR).

2.5 Cold spot conditions

To find out whether cold spots conditions are present in each limb profile have some conditions are taken.

- The surface temperature is less than 140 K . As stated in multiple papers, the conditions for the cold spot is Tb (Brightness temperature 22.2 μm) <148 K (Kieffer et al., 1976). It is possible to take Tb nearly equal to surface temperature because of two reasons.
  - ❖ Brightness temperature (from channel 22.2 μm) is used as a measurement function for temperatures 0-20 km. From table 1.

$$Tb = \epsilon T \quad \text{(eq-1)}$$

  where Tb is brightness temperature, ϵ is emissivity and T is surface temperature.

  - ❖ From Figure 1 in (S. W. Ruff et al., 1999 ; P. R. Christensen et al., 1999) “Bibcode: 1999ficm.conf.6230R ” paper. It is found that the range of general emissivity of the surface lies from 1 to 0.7 (which can be taken as nearly equal to 1). So the surface temperature is taken from the DDR datasets.

- The vertical temperature point is less than the CO_2 frost point line. It will provide a general idea of finding the heights below the CO_2 frost point which support the formation of CO_2 ice clouds (Neumann et al., 2003; McCleese et al., 2008). The CO_2 line in the graph was extrapolated from Figure 9 from the paper (https://doi.org/10.1029/2011JE004040). Used a simple line equation as the line is linear up to 30 km. This CO_2 is nearly accurate up to 40 Km martian height. Can use pressure surface in replacing to height to give better results.

$$Y = m X + C \text{ (line equation)}$$

$$T_{co2} = (\text{Height-30km}) *(-5/6))+120K \text{ (} CO_2 \text{ frost temperature line equation, eq-2).}$$

- Also restricted profile height up to 40 Km. Saturation with respect to CO_2 does not typically occur above 30 or 40 km, consistent with the polar winter middle-atmosphere warming (inversion layer) reported by (McCleese et al ., 2008).

2.6 MCD Reanalysis data

The datasets from the Mars Climate Database (MCD) used for understanding the Martian climatic system and its key components like stability profile and surface ice change. MCD has the Martian meteorological data simulated from the LMD Global Circulation Model. The MCD data contains reanalysis data with multiple scenarios like the average climatology, real scenario, maximum dust scenario, and low dust scenario data from Martian years 24 to 33.

3. Cold spots properties MY 33 vs 34

3.1. Martian dust storm years vs non-dust storm year (Stability profile around ~Ls 207^o)

From the Figure 2 it shows the potential temperature gradient increase with respect to the altitude at the region of ~ 30-40 km at ~ 20^o N - 90^o N (magnitude 4 contour line) due to extra-tropical baroclinic conditions around ~ 30^o N to 60^o N (sudden rise of meridional temperature gradient) (Haberle et al., 1982; Barnes et al., 1984). This leads to the inversion layer in the winter hemisphere. The reason for the presence of the inversion layer in much of the northern mid-latitudes and subpolar region is due to compressional heating associated with the descending branch of the Hadley circulation (Haberle et al., 1982). During the dust storm years in Figure 2b It is seen that the red line (maximum extent of magnitude 6 K/km contour line) is near 30 km wherein in Figure 2 it is near 24 km. This means in the global dust storm season the stable atmospheric conditions in present at higher levels of the troposphere. Thus saturation concerning CO_2 does not typically occur above ~40-30 km in the atmosphere, consistent with the polar winter middle-troposphere warming or inversion layer (McCleese et al., 2008) and the presence of a dust concentration in the atmosphere during dust storm year, which heats up the atmosphere, enhances the static stability of the atmosphere in ways not dissimilar to water vapor in Earth's humid atmosphere (Haberle et al., 1982; Schneider, 1983). This helps us to know the limits where the vertical temperature will fall below the CO_2 frost line and hence form polar clouds that help in the generation of cold spot regions. Hence it can be summarized

- There is an extratropical inversion layer during winter.
- During the dust storm season, higher altitude becomes more stable.
- Thus inversion layer causes a stability region that generally inhibits the formation of CO_2 ice or polar clouds above it (~ 30-40 km).
- Thus it is possible to find more aerosols particle at higher altitudes in the global dust storm season as compared to the non-dust storm season.

Stability criteria:- From the vertical temperature profile and pressure profile. The general stability condition of the Martian atmosphere can be derived. The vertical Potential temperature gradient is of great significance since profiles of θ indicate the static stability of the air.

$$\theta \equiv T \left(\frac{P0}{P}\right)^{R/Cp} \quad \text{(Poisson equation, eq-3)}$$

Here, P0 is the martian average surface pressure, R is the specific gas constant, and Cp is the specific heat at a constant pressure of the gas mixture. For Mars, R is 188 J Kg^{-1} K^{-1}, P0 is 660 Pa and Cp is 730 J K^{-1} Kg^{-1}. Initial results suggest that for.

- If $d\theta/dz < 0$, then air is unstable, supporting the rising motion.
- If $d\theta/dz = 0$, then neutral condition.
- If $d\theta/dz > 0$, the air parcel is highly stable.

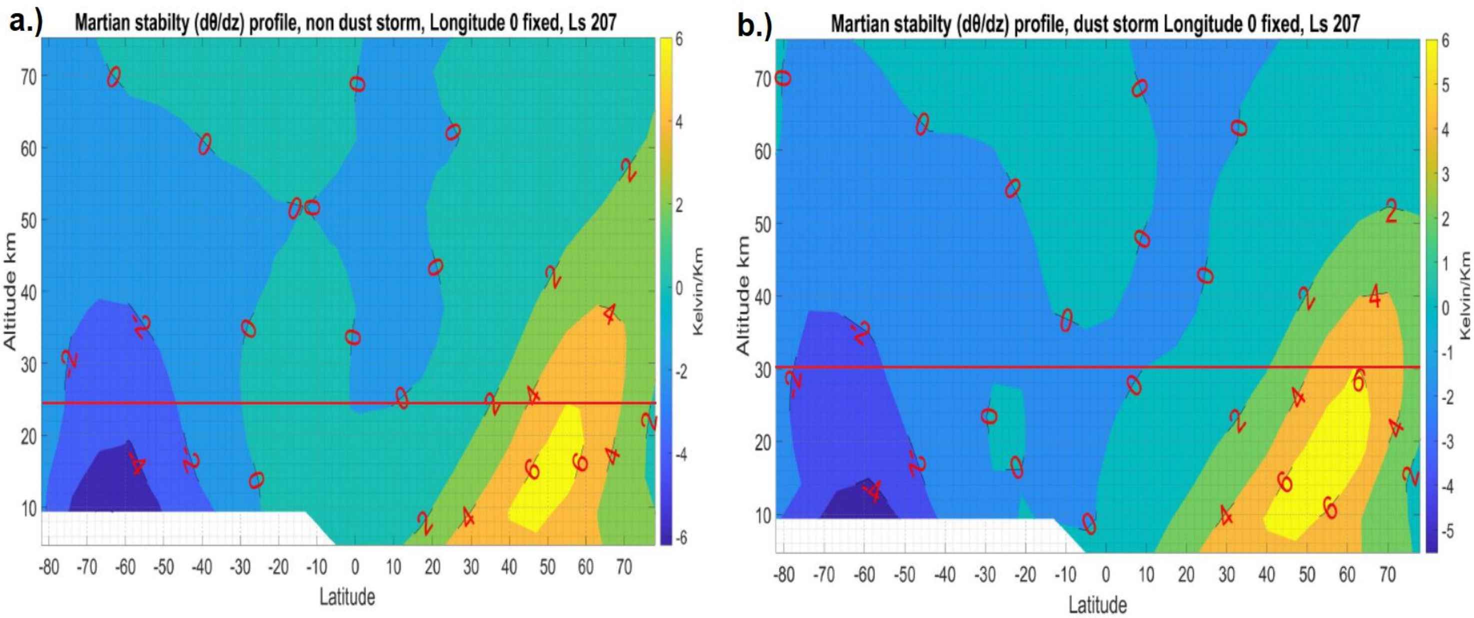

Figure 2. Shows vertical stability profile plot comparing both dust storm (average) and non-dust storm years. (MCD reanalysis data, (Forget et al., 1999 ; Millour et al., 2018))

3.2 Martian year 33 vs 34. (Areocentric Longitude Ls vs Latitude)

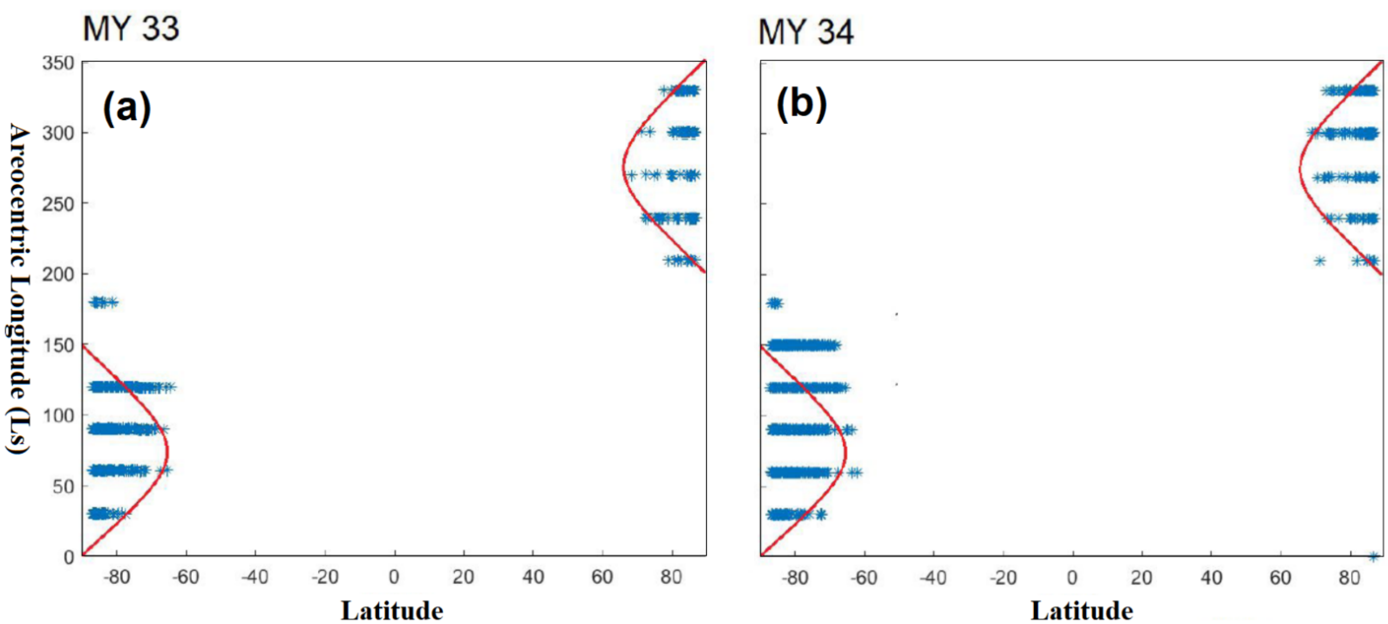

Figure 3. Describes scatter plot variation of cold spot regions (Places where the Surface temp is less than <140 K and in vertical temperature profile having a point less than CO_2 frost point line). It shows the seasonal variation of cold spots. Have taken Ls 30 bin Martian 1 year data. Redline gives us the extent of the polar night. (Ls 30 bin, 1 Martian year data).

From Figure 3 the latitudinal variation of cold spot regions can be observed with respect to seasonal variation. Cold spot regions shift their latitudinal polarity with respect to seasonal change. That means a cold spot in the southern hemisphere is prominent in southern winter and the same goes for the Northern hemisphere. This shows a direct link with seasonal change in solar insolation (James et al., 1992). The prominent difference between the south and north cold spot regions was that in southern cold spot regions have their dominance of the outer-polar ring (~ > 80° N/S). Hence southern region's outer polar ring shows more activity than the north. This is visible in the scatter plot as scatter point distribution in the south -90° S to -60° S is more than north 60° N to 90° N. Most of the southern hemisphere cold spot regions are formed within the polar night (Figure 3, inside red curve), also it is similar to those in the north (Cornwall and Titus, 2009). Cold spot regions outside the polar night (red curve) in the southern hemisphere are more common than the cold spots that occurred outside the polar night in the northern hemisphere. The Viking IRTM data studies suggested northern hemisphere cold spots were more common at low latitudes (Forget et al., 1995). These observations were a bit counterintuitive because the extent of the polar cap is larger in the south. From the TES data studies observed that the southern hemisphere cold spots occurred at much lower latitudes and they were more frequent in the low latitudes compared to the northern hemisphere which can be due to old extensive terrain surface (Cornwall and Titus, 2009). The TES data study is supported here by the Figure 3 plot done using MCS DDR data sets. In the northern hemisphere, the cold spots that are present outside the polar night were closely tied to terrain or topographic-induced cold spots (Cornwall and Titus, 2009). In Figure 3b it is observed that scatter points are more in number in MY 34 from ~ Ls 150° – 350°. That means an intensification of outside polar night cold spots in the southern region around Ls 150° is observed. Which is around the very early stage of the dust storm. While in north scatter point intensification is visible and around ~Ls 200°, MY 34. It can be seen that scatter point at low latitude as compared to its MY 33 counterpart. Summarizing time of dusty atmosphere (MY 34) would experience greater cooling within the polar night, resulting in enhanced atmospheric condensation, which could explain the increase in scattering points in Figure 3b. It can also be seen in Figure 3b that there are many scatter points in ~Ls 300° to 330° which states that the cold spot activity increased after dust storm passage to multiple factors than that of the previous non-dust storm year.

Hence, it can be summarized.

- Southern non-polar night cold spot regions are more dominant than northern cold spots regions.

- Southern cold spot regions extend to lower latitudes as compared to their northern counterparts.
- During global dust storm MY 34 year, the overall cold spots regions are intensified.
- During global dust storm MY 34 year, the nonpolar night cold spot regions have more intensification as compared to MY 33.
- During global dust storm MY 34 year , it is observed the progression of nonpolar ring cold spots regions or low latitude cold spot regions in the northern hemisphere as compared to MY 33.
- A spike in cold spot activity in the northern hemisphere after the dust storm passage in MY 34 as compared to its counterpart MY 33.

3.3 Martian year 33 vs 34. (Vertical Temp vs Altitude)

In Figure 4 it is directly seen that there is more intensification of scatter points in MY 34 as compared to M33. Also, it is seen that the median line for MY 33 is 15.5 km, and for MY 34 median line is 14.05 km. Which shows a decrease in the median line and states vertical temperature scatter plots decrease in height in dust storm year M34. This is due blocking of solar insolation by the dust particles in the air causing a low attitude and a near-surface cooling effect (James et al., 1992). Also in Figure 4b scatter plot, it can be visualized that many scatter points have low temp as compared to MY 33 plots. Hence supporting the above dust cooling theory. Also, the scatter points are more lifted up in MY 34. It can be seen that more scatter points are above or near 30 km. It can be explained that during the dust storm year inversion layer or stability layer increase to a higher height, Figure 2b. Knowing vertical temperature points distribution lesser than CO_2 frost line gives us an idea of possible or suitable location for CO_2 ice clouds (Neumann et al., 2003; McCleese et al., 2008). Hence, the following aspects can be drawn from the analysis:

- More vertical temperature profile points below the CO_2 frost point are prominent in MY 34 global dust storm year.

- The more vertical temperature profile points that reach below the CO_2 frost point are at a lower altitude in MY 34 as compared to MY 33.
- In MY 34 the vertical temperature profile points reach a more low temperature as compared to MY33.
- In MY 34 the vertical temperature profile points that reach below the CO_2 frost point is situated at higher altitude (≥ 30 km) as compared to MY 33.

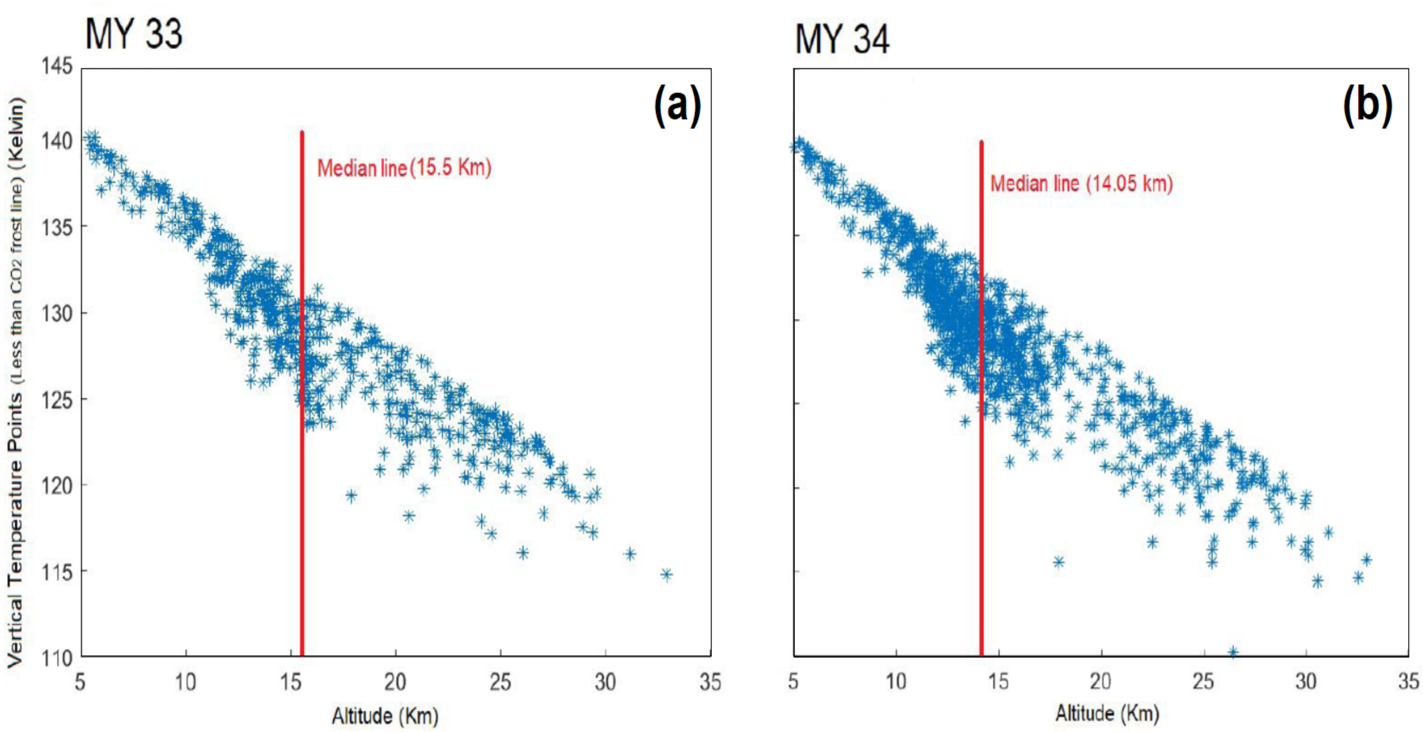

Figure 4. Show scatter plot of Vertical temperature points that satisfied the "less than" condition with respect to the vertical CO_2 frost point line. There is a median line that states most of the scatter points lie. (Ls 30 bin, 1 Martian year data).

3.4 Martian year 33 vs 34. (Dust opacity per km vs Altitude)

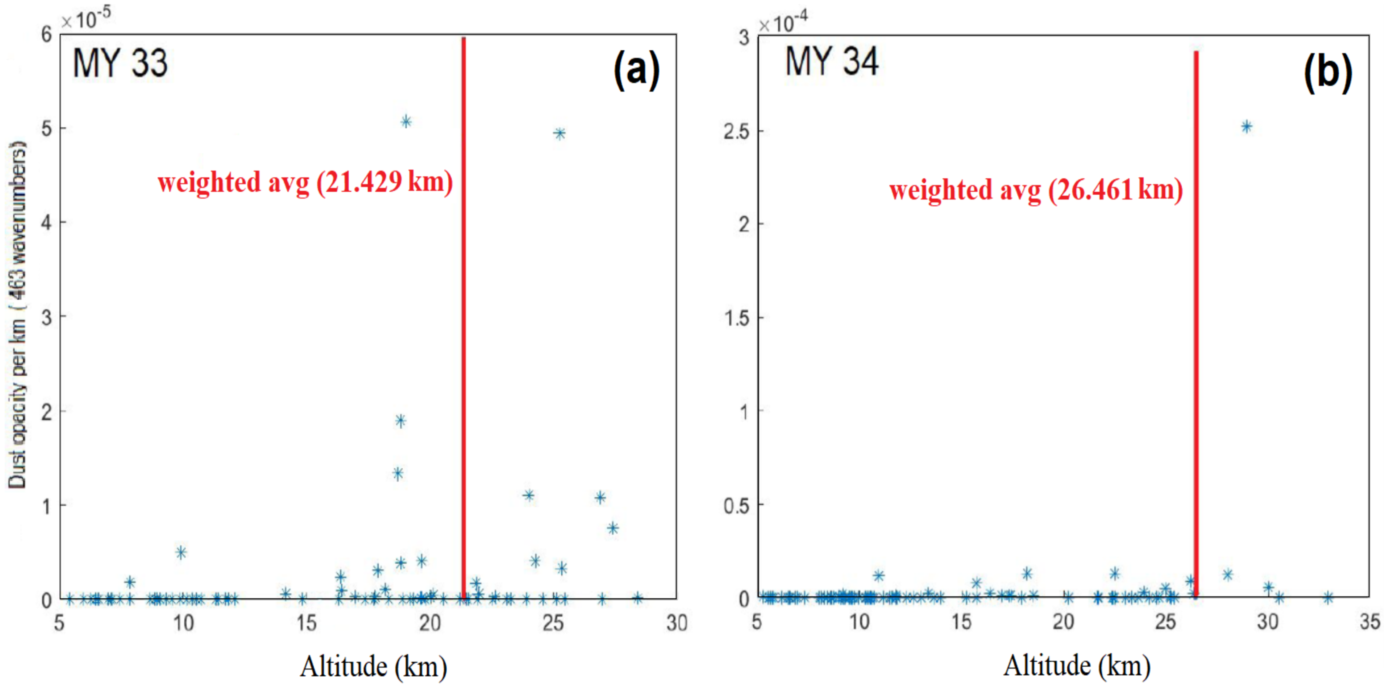

Figure 5. Show scatter plot Dust opacity per Km (That satisfied cold spot profile condition) vs Altitude. There is a weighted function value line that states most of the scatter points lie. (Ls 30 bin, 1 Martian year data)

In Figure 5, it can be can seen that the weighted average line for MY 33 is 21.429 km and for MY 34 is 26.461 km.

$$\text{Weighted average} = \frac{\sum f(a)g(a)}{\sum f(a)} \quad \text{(eq-4)}$$

In the above Figure 5 it can be seen that in both of the figures the scatter points have low dust opacity per km value in MY 33 and M34 the overall cold spot formation due to dust is less as the global dust storm is confined to Ls 180^{o}-330^{o} but it also states that dust opacity per km of cold spot profiles increases in height. From the weighted average line, it can be seen that in MY 34, the dust activity is at a higher altitude as compared to MY33. The dust abundance and height are enhanced by dust lifting and deep convection, but the impact of dust is less at higher latitudes than at mid-latitudes (Heavens, N. G. et al., 2018). Also, dust acts as a nucleation site for ice and further drives CO_2 ice clouds formation which are similar to terrestrial cirrus clouds (Gooding et al., 1986). It is related to many microphysical processes, including heterogeneous nucleation. Higher dust activity blocks solar insolation and this is the reason for lower vertical temperature profile points in Figure 4b. Hence, it can be summarized.

- The overall yearly impact of dust in the formation of the cold spot region is minor but still impactful.
- Dust opacity per km of cold spot profiles has a higher value in MY 34 as compared to MY 33. The obvious reason is that MY 34 is a dust storm year.
- There is more dust lifted up in higher latitudes in MY 34 as compared to MY 33.
- This causes lower vertical temperature. As shown in Figure 4b.
- Dust encourages the formation of clouds.

3.5 Martian year 33 vs 34. (Water ice opacity per km vs Altitude)

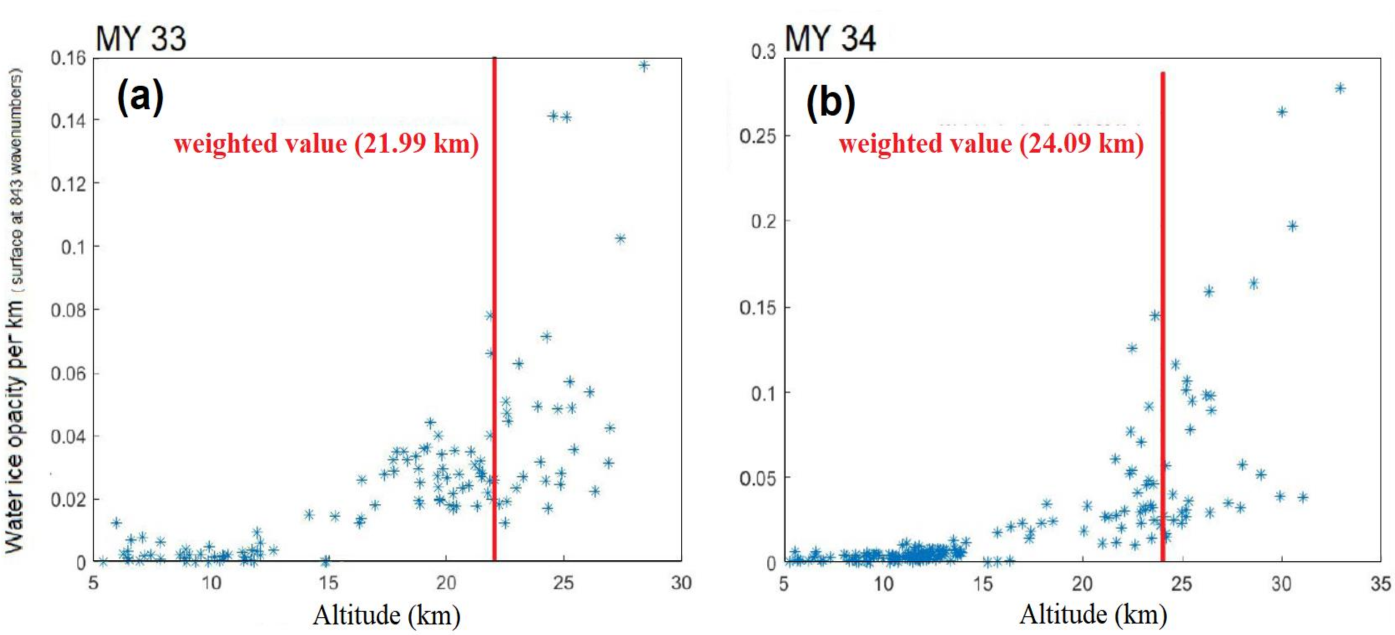

Figure 6. Show scatter plot water ice opacity per km (That satisfied cold spot profile condition) vs Altitude. There is a weighted function value line that states most of the scatter points lies. (Ls 30 bin, 1 Martian year data)

In Figure 6, water ice opacity per km of cold spots regions can be observed to increase in MY 34 as compared to MY 33; also it can be seen that the ice opacity per km has a higher value in higher height levels (~ ≥ 20 km). The height weighted average value line in Figure 6b is 24.09

km as compared to Figure 6a is 21.99 km. Which is correlated with Figure 5. As higher dust particles in a higher atmosphere provide suitable conditions for heterogeneous nucleation (Gooding et al., 1986). This also provides suitable conditions for the formation of CO_2 ice with the water ice and dust contaminants nucleation sites under CO_2 frost points, thus stating the possible presence of polar clouds. Although many research studies show CO_2 ice generally starts to form below dust and water ice concentration maxima as water freeze point is generally higher than CO_2 (Hayne et al., 2012). Hence, it can be summarized.

- MY 34 cold spot regions show more water ice presence in the atmosphere as compared to MY 33.
- MY 34 cold spots regions show higher altitude water ice opacity per km as compared to MY 33.

3.6 Martian year 33 vs 34. (Surface Temp vs Latitude)

In Figure 7 it can be seen that scatter points in general in the south are more as compared to the north which is supported by the Figure 3 plots. Here the visible differences is that in the plot between MY 33 and MY 34 that in Figure 7b plot, inside the ~ 130-140 K (y-axis) and 60° - 80° N (x-axis) has slightly more scatter points than its MY 33 counterpart. This is more clearly visible from Figure 8a and 8c in the regions greater than 80^{o} N (x-axis) and also through the median line difference from Figure 9. These can be due to the blocking of solar insolation in lower latitudes or outer polar circle regions, which in return causes favorable cold spot region conditions (James et al., 1992). This is also visible in the southern hemisphere in MY34 outer polar circle region cold spots are more. Also, temperature scatter points in Figure 7b and 8d, 8c has lower temperatures ~ < 115 K values as compared to Figure 7a., 8a and 8b. The most noticeable difference between the north and south cold spots was that in south region exhibited approximately three times as much cold spot activity outside the polar ring as compared to north region. While in the plot it is the evident tropical region has no cold spot region conditions.

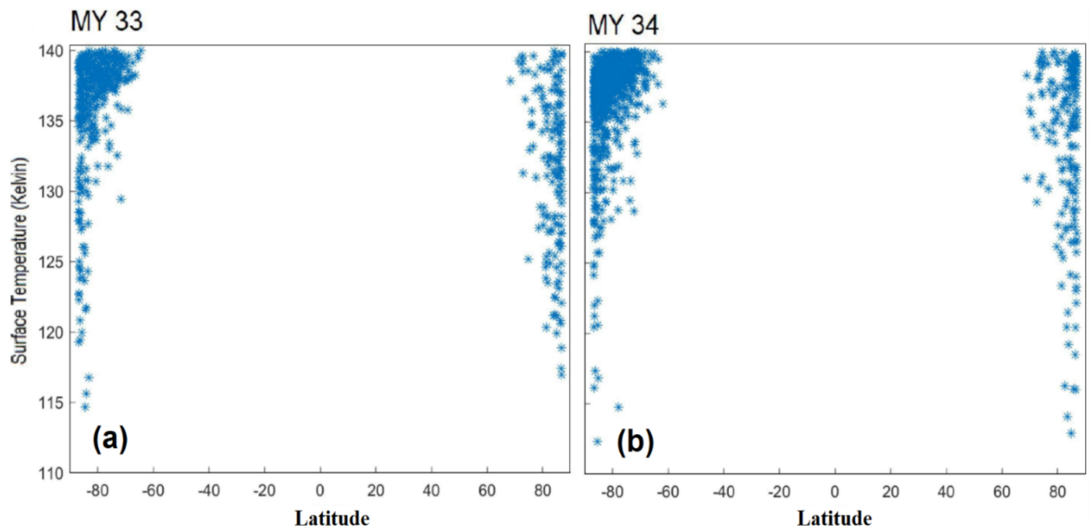

Figure 7. Shows scatter plot of Surface Temperature that satisfied the “less than” condition with respect to surface CO_2 frost point ~140 K with respect to latitude. (Ls 30 bin, 1 Martian year data)

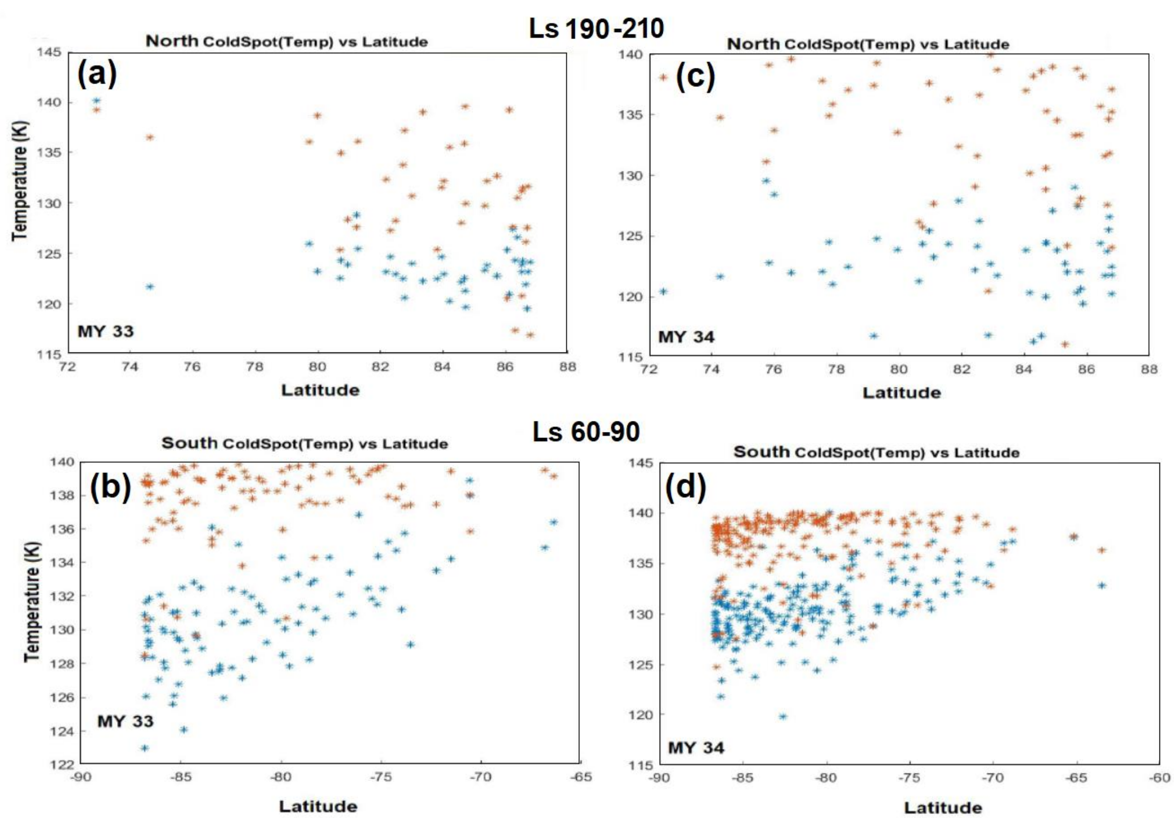

Fig 8. Shows scatter plot of Martian latitude with respect to Surface Temperature and Vertical temperature and compares with North (a, c) vs South (b, d). (While “* red” is for Surface Temperature and “* blue” is for Vertical Temperature points that satisfied the “less than” condition with respect to the vertical CO_2 frost point line).

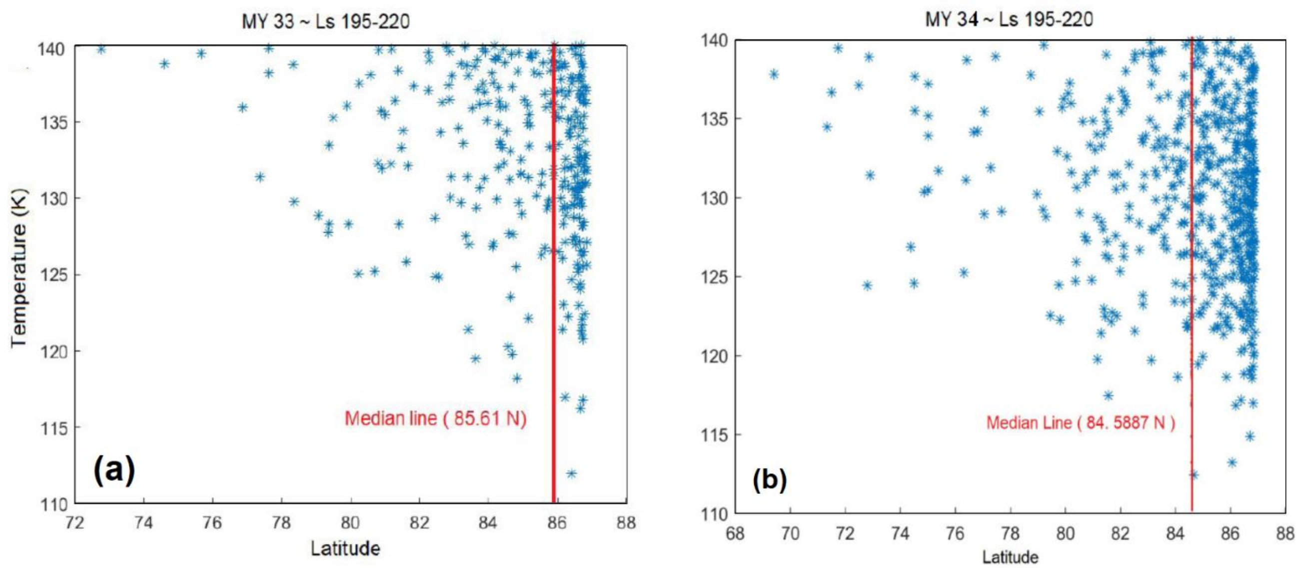

Figure 9. Shows scatter plot of Martian latitude with respect to Surface Temperature (that satisfied the “less than” condition with respect to surface CO_2 frost point ~140 K) .

In Figure 8, it can be seen that the similar general trend is present in Figure 7. But here it provides more clear representation and division of southern hemisphere and northern hemisphere cold spot regions and its respective vertical temperature regions. In Figure 9, the data during the dust storm peak (MY 34, ~ Ls 207^{o}) has taken and compared it with its MY 33 counterpart. It is visible that the median line for MY 34 (84.5887^{o} N) is less than MY 33 (85.61^{o} N). Hence the during the early to peak dust storm non-polar cold spots are more than MY 34. Also, cold spot region distributions shift to lower latitude. Which is supported by Figure 7 and 8.

Hence, it can be summarized.

- In MY 34 north regions has more cold spots regions outside of polar circle as compare MY 33.
- In MY 34 also southern regions has more cold spots regions outside of polar circle as compare MY 33.
- Southern hemisphere cold spots regions outside of polar circle is more as compared to its northern counterpart.
- Temperature of cold spot regions decreases in MY 34 as compared to MY 33.
- Cold spots regions do not form near tropical regions.

3.7 Martian year 33 vs 34. (LTST vs Surface Temp)

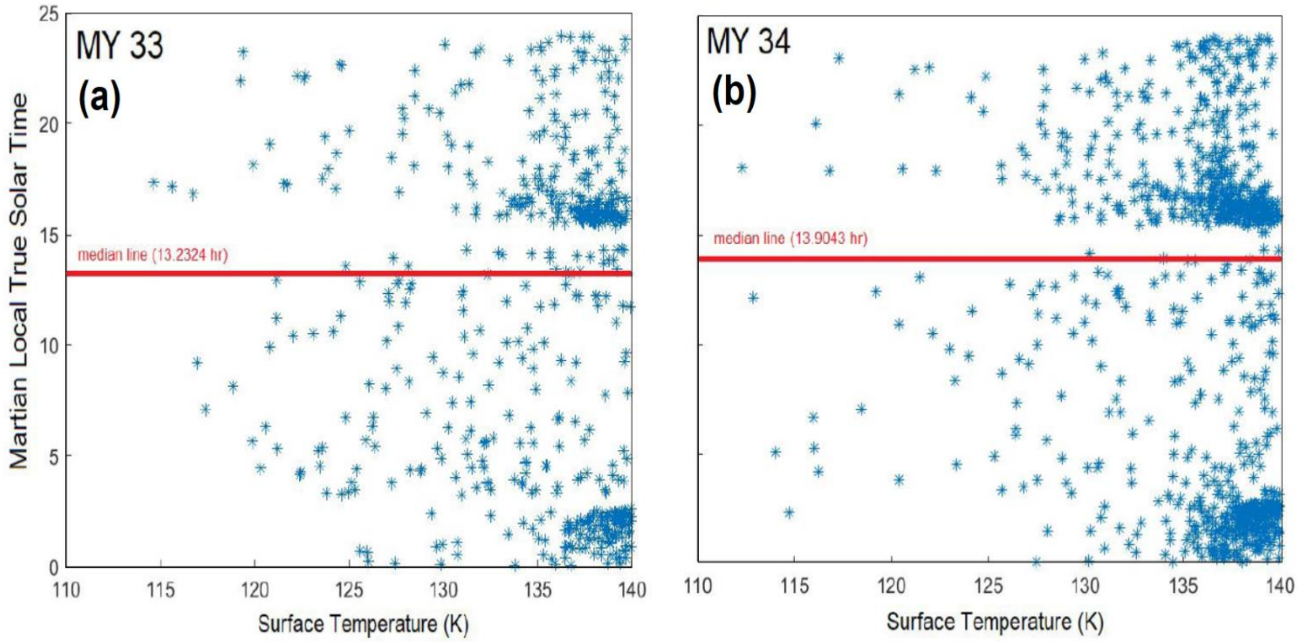

Figure 10. Shows scatter plot of Martian Local time with respect to Surface Temperature that satisfied the “less than” condition with respect to surface CO_2 frost point ~140 K.

Through the Figure 8 plot it can be can seen that a bipolar distribution of scatter plots is present around 15-20 hr and 0-5 hr LTST (Local True Solar Time) which it falls during sunset and early morning. While the rest one is formed during polar night. The southern polar nights are longer than norther polar night due to southern winter lies in aphelion. On earth it is normally observed that, during long polar night, 24- hour periods darkness with a clear sky and light to moderate winds have their lowest temperatures in the middle of the period, and the highest temperatures occur at the beginning and end. But the net diurnal change is minimum (Barrigar et al 1963; Donald et al., 1963). The early morning distribution one indicates cold spots formed during non-polar night. As during the dust storm year MY 34 due to low solar insolation there more formation of cold spots especially non-polar night cold spots which in turn increase the median line value in Figure 10b.

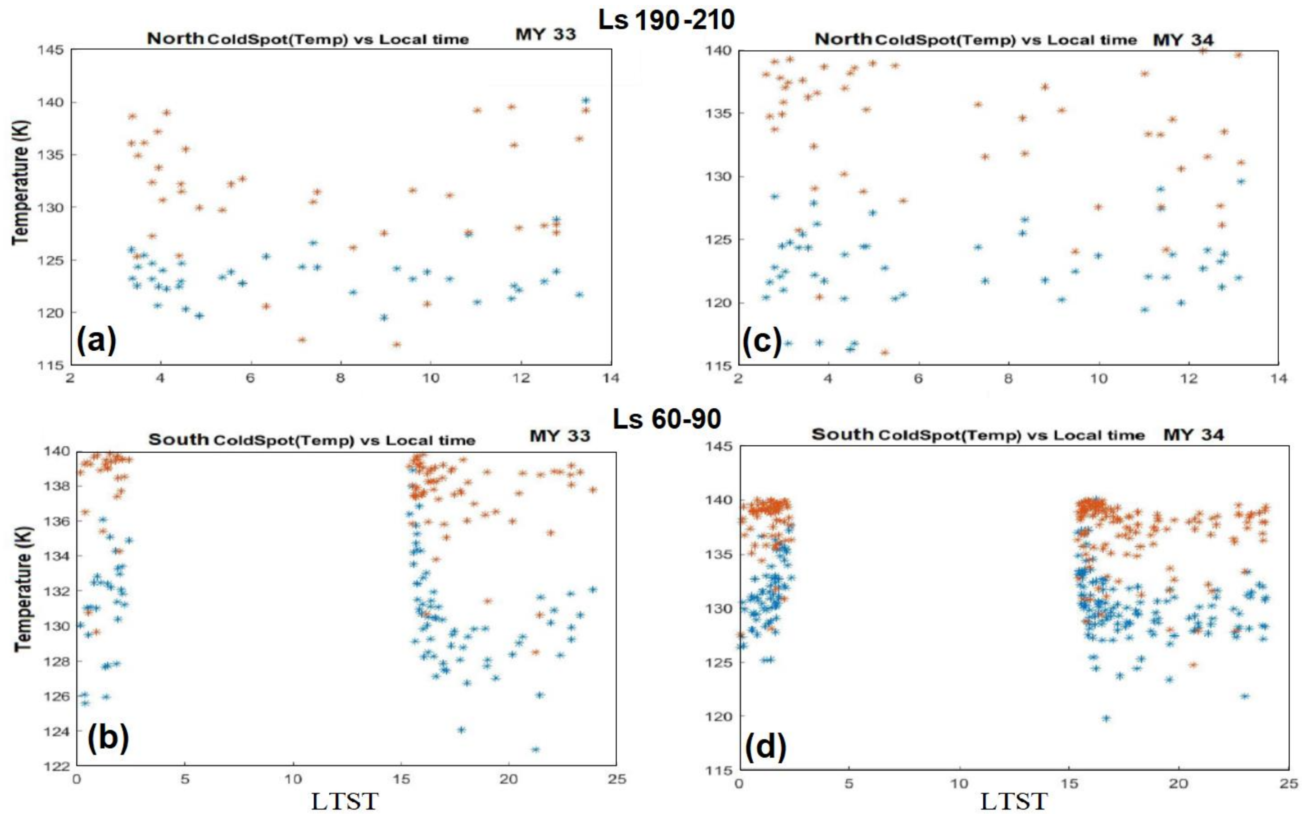

Figure 11. Shows scatter plot of Martian Local time with respect to Surface Temperature and Vertical temperature and compares with North (a, c) vs South (b, d). (While "* red" is for Surface Temperature and "* blue" is for Vertical Temperature points that satisfied the "less than" condition with respect to the vertical CO_2 frost point line).

Here in Figure 11 it can be seen that for northern hemisphere diurnal variation of scatter points are minimal. Which states polar night cold spot regions are common in northern hemisphere as compared to southern counterpart. Which also supported by study in Figure 3. While in south there is bipolar distribution of scatter plots which also influence scatter points in Figure 10. In Figure 11c, around 2-6 hr (LTST) it is seen more scatter points as compared to Figure 11a, which states generation of non-polar night cold spots as discussed in Figure 3 section. While there is no cold spot region formation in 5-15 hr (LTST) in southern hemisphere. Hence, it can be summarized.

- In north it is seen that polar night cold spots are common as there is less diurnal variation.
- Formation of non-polar night cold spots in northern pole during MY 34-dust storm year.
- There is a bipolar diurnal distribution of cold spots region in the plot for southern

hemisphere region.

3.8 Martian year 33 vs 34. (Temperature, Dust opacity, Ice opacity and its variation)

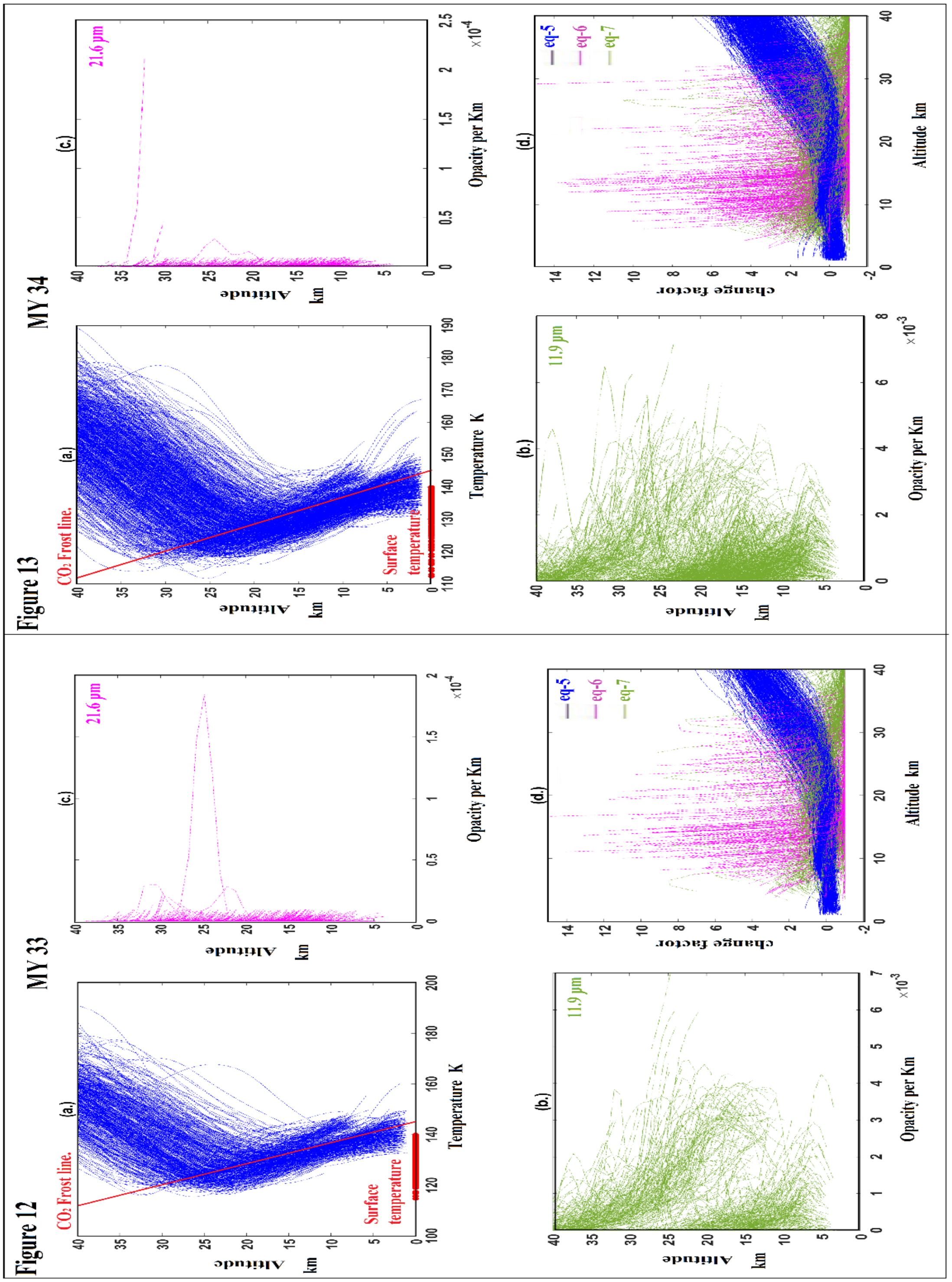

Figure 12 (MY 33) and 13 (MY 34). Shows vertical temperature profile (a), ice opacity per km (b), dust opacity per km (c) and correlation plot (d). Comparing both dust storm MY 34 and non- dust storm years MY 33.

From the Figure 12 and 13 it can be derived a correlation between cold spot regions, temperature, In Figure 12a and 13a it can be seen that there is a presence of a red line. This red line is CO_2 frost line derived from equation (eq-2). The vertical temperature curve line below CO_2 frost line gives the possible region of CO_2 saturation and frost formation. In Figure 12b and 13b gives ice opacity per km while in Figure 12b it is visible that there is rise of ice opacity per km in higher altitude due to dust acts nucleation sites for heterogenous nucleation during dust storm year. This helps us to find possible height of polar clouds. In Figure 12c and 13c gives dust opacity per km while in Figure 13c there is dust opacity per km rise due to dust storm year. In Figure 12d and 13d provide a correlation. In the figure there is a trend which states low temperature change value and in high dust change line provide the region for maximum ice change line. Hence during dust storm dust change peak is at higher altitude and temperature change is lower value at higher altitude. Causes ice formation in higher altitude. Which supports study in Figure 4, 5, and 6.

As the change of each variable is plotted against with each other.

Temperature change factor= $\frac{(Temperature\ of\ each\ profile)-(CO2\ frost\ point\ temperature)}{(CO2\ frost\ point\ temperature)} \times 10$ (eq-5)

D.O per km change factor = $\frac{(D.O\ per\ km,each\ profile)-(D.O\ per\ km,MEAN)}{(D.O\ per\ km,MEAN)}$ (eq-6)

I.O per km change factor = $\frac{(I.O\ per\ km,each\ profile)-(I.O\ per\ km,MEAN)}{(I.O\ per\ km,MEAN)}$ (eq-7)

D.O = dust opacity (τ); I.O = ice opacity (τ).

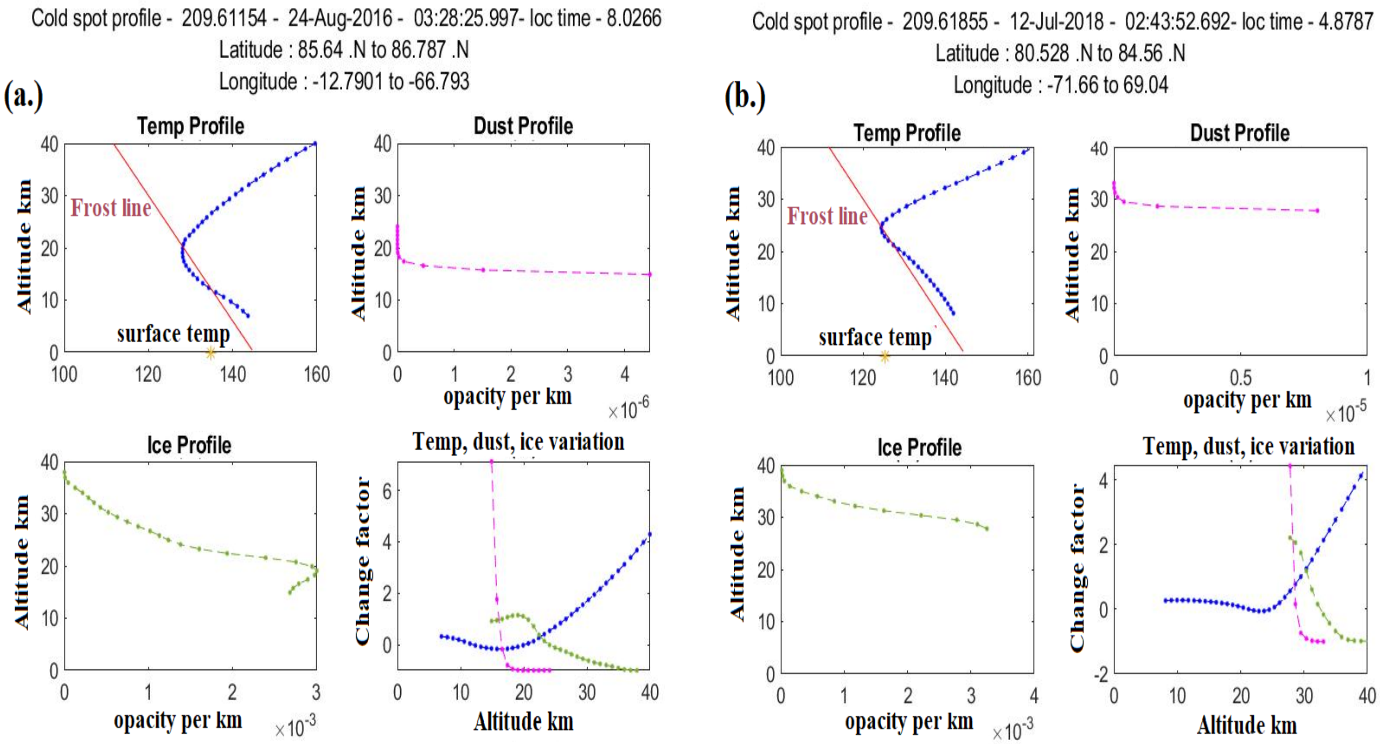

Figure 14 shows (a.) MY 33 and (b.) MY 34. Shows each specific cold spot limb profile present in compilation plots of Figure 12 and 13. In correlation plot, red line is D.O per km change factor, yellow line is I.O per km change factor and blue line is Temperature change factor.

Figure 14 is a simpler illustration of specific cold spot regions and could be quite helpful in understanding the results demonstrated in Figures 12 and 13. The Figure 14 variation plot section clearly shows that during dust storm water ice and dust concentration are generally at higher altitude. With lower temperature change factor gives possible location of polar clouds.

Hence, it can be summarized.

- Positive correlation between D.O per km change factor with I.O per km change factor.
- Negative correlation between I.O per km change factor with temperature change factor.
- Higher D.O per km change factor value with higher I.O per km change factor and lower temperature change factor gives possible polar cloud condition and CO_2 clouds. That satisfies third cold spot formation hypothesis by polar clouds.

3.9 Martian year 33 vs 34 (Spatial Plots, North pole (~Ls 195º – 220º))

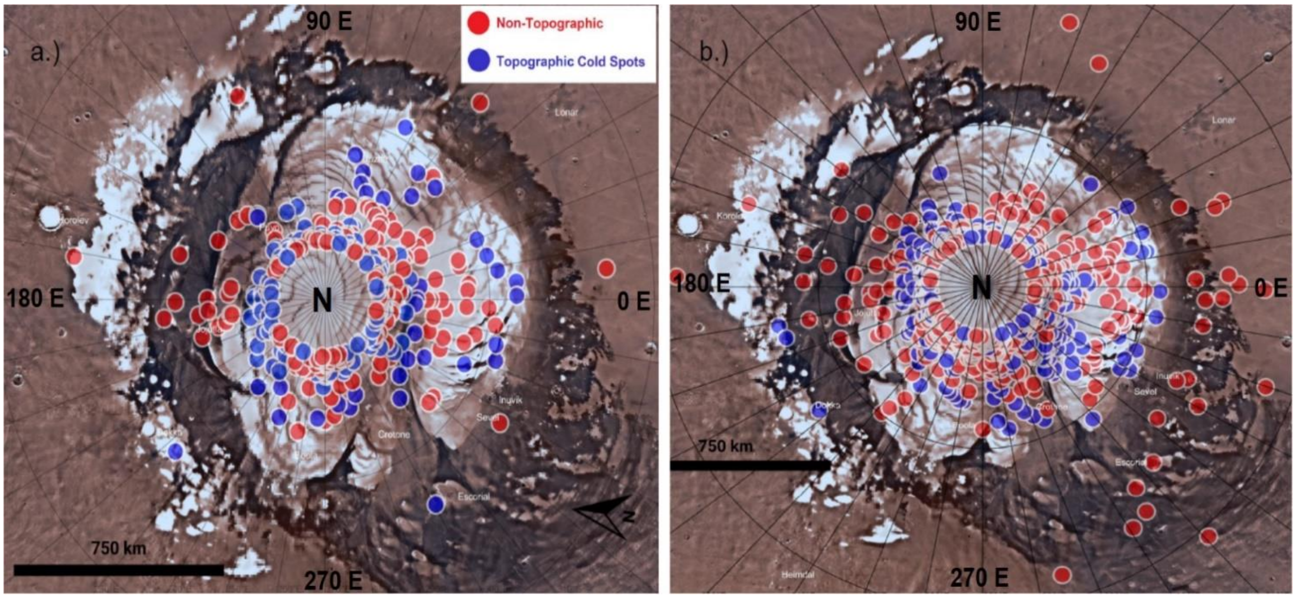

Figure 15. Shows spatial pots of possible cold spots region for MY33 and MY (~Ls 195º – 220º). Red point is due to non-topographic induced cold spots and blue due to topographic induced cold spots. This found by plotting point data on MOLA terrain map and find out valley and crater regions for topographic cold spots.

In the Figure 15, it can be seen that the spatial plot of topographic and non-topographic cold spots was derived by plotting gridded cold spot regions data on the MOLA, JMARS terrain map. Retrieval of South pole topographic and non-topographic cold spots is difficult especially for the outer polar circle regions due to extreme and old uneven high terrain features. In MY 33, Figures 15a and 16a, there is a near equal distribution of topographic and non-topographic cold spot regions. In MY 34 there is a decrease in topographic cold spot activity as compared to MY 33. This may be due to the suppression of the processes that cause CO_2 snow formation through orographic lifting or gravity waves which caused adiabatic expansion of air parcel thus cooling. There is a reduction of solar insolation due to the suspended dust particles in the atmosphere which may reduce the wind speeds (weakens polar jet streams) necessary to form topographic cold spots. It is also possible that snow formation was impeded because of near-surface atmospheric heating caused by an expansion of the Hadley cell can be seen by the expansion of the inversion layer in Figure 2. (Wang et al., 2007). Also, a dust-filled aerosol atmosphere would have a greater cooling effect during the polar night, resulting in the increase in atmospheric condensation, which might explain the increase in non-topographic cold spot formation during the early dust storm period (Ls ~195o-210o) (Pollack et al., 1990; Forget et al., 1998). Increased dust concentration in the atmosphere near the polar regions would also increase the rate of formation of CO_2 clouds (Pollack et al., 1990) because dust particles are effective nuclei for snow formation (Pollack et al., 1979; Neumann et al., 2003; McCleese et al., 2008). This might also explain the increase of non-topographic cold spot activity near the lower latitude in MY 34, Figure 15b and overall, in MY 34 region as compared to MY 33.

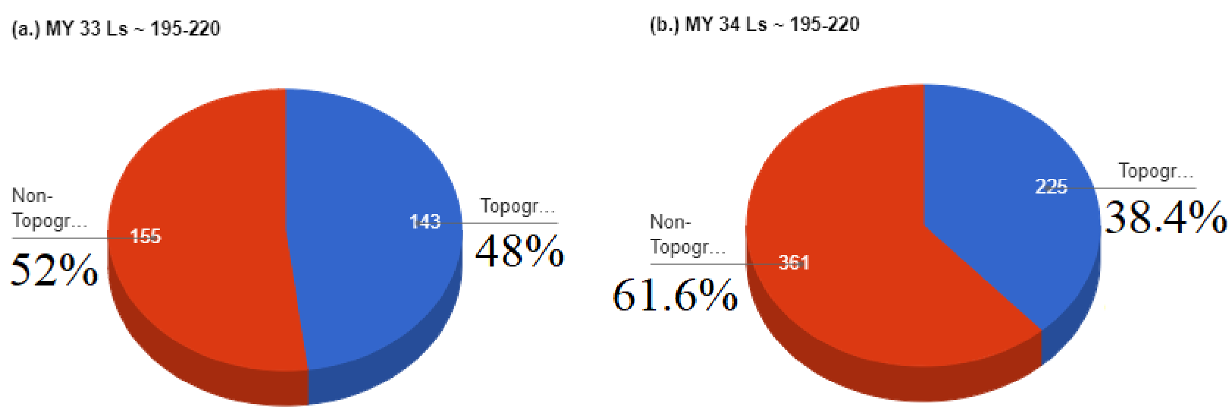

Figure 16. Pie charts shows the percentage change of topographic and non-topographic cold spots region for MY33 and MY34. Red is non-topographic and blue is topographic cold spot regions (~Ls 195 - 220).

In the Figure 16 that shows pie chart, it is observed that in MY 33 ~Ls 195°-220° has 52% non-topographic cold spot regions and 48% topographic cold spot regions. While for MY 34 ~Ls 195°-220° has 61.6% non-topographic cold spot regions and 38.4% topographic cold spot regions. Which supports the studies and discussion done in Figure 15. Hence, it can be summarized.

- During the MY 34 global dust storm, the non-topographic cold decreases in northern hemisphere as compared to MY 33.
- During the MY 34 global dust storm cold spots regions in northern hemisphere starts forming in lower latitude as compared to MY 33.
- During the MY 33 year the distribution of topographic to non-topographic is nearly equal

3.10 Ice H_2O and CO_2 change anomaly. (kg/m^2 vs Areocentric Longitude)

In the Figure17 the diurnal average is taken instead of zonal average also Longitude at 0 is fixed because in Figure 13 it is visible that during dust storm year MY 34 cold spots starts forming in lower latitude near 330^o E to 30^o E longitude. MY 25 and 28 data average is taken as in MCD reanalysis datasets MY 34 data is not available. Then difference of Dust average with non-dust storm year (MY 33) is taken.

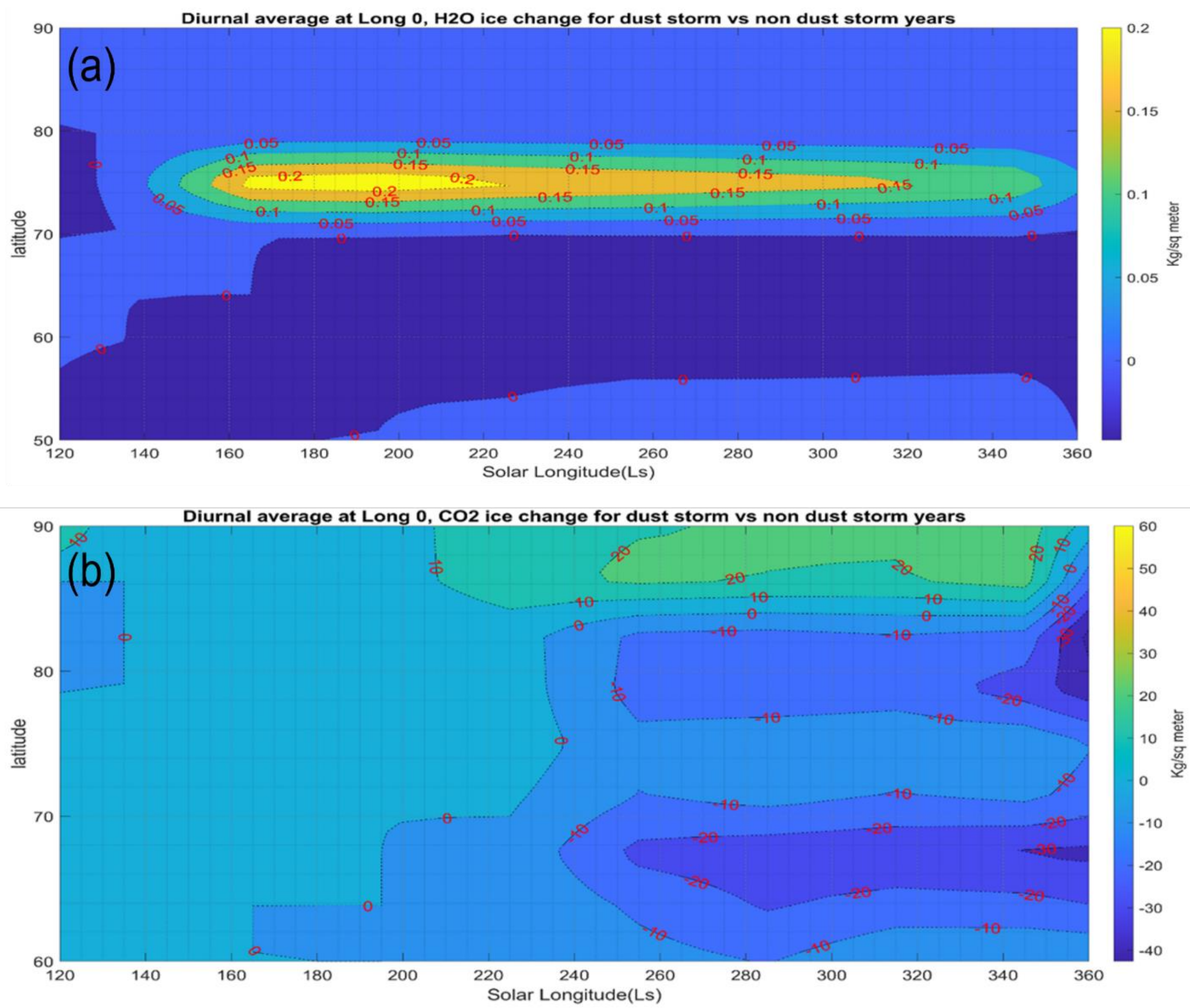

Figure 17. Shows Hovmoller ice change (~Ls 120^o- 360^o, region of interest). (a.) depicts H_2O ice change and (b.) depicts CO_2 ice change diurnal at Longitude 0. The results are obtained using the MCD reanalysis data set.

As in Figure 17a, it shows during the Ls 207^o peak dust storm month the ice change is positive or maximum inside 80^o-70^o N which also falls in the region of Figure 15b region of outer polar ring (80^o N) cold spots regions. While Figure 15b around Ls 207^o this region shows negligible dry ice change the regions above ~85 ^{o} N shows positive change which states maximum dry ice growth. These combined plot shows the during dust storm year there is ice cap growth around Longitude 0^o E. Where dry ice growth is also increased during dust storm year. This correlated with the cold spot regions growth with lower latitude in Figure 15b.

Hence, it can be summarized.

- During the global dust storm year there is positive water ice growth in lower latitude of northern hemisphere.
- During the global dust storm year there is negligible dry ice growth in lower latitude of northern hemisphere.
- During the global dust storm year there is positive dry ice growth in higher latitude above ~85 ^{o}N.
- During the global dust storm year water ice growth directly correlates with cold spot regions growth in lower latitude.

4. Conclusions and future scope

Global dust storm affects the latitudinal variation in the formation of ice caps and lower solar insolation, which in return impacts the cold spot region formation. Global dust storm increases the stability of higher altitude (Figure 2). In the south pole, cold spot regions are more dominant than in the north pole, especially in non-polar ring regions (Figure 3). It is found that most North Pole cold spots form on the polar night (Figures 3 and 11). During the global dust storm season, the cold spot regions in the northern hemisphere start to form outside of polar ring regions (Figures 8, 9, and 11). It is also seen that during dust storms there is a high concentration of dust at higher altitudes which in return provides a nucleation site for water vapor and dry ice to form polar clouds (Figures 5 and 6). Have also formed a correlation with the variation of vertical temperature change, D.O per km change, and I.O per km change with surface temperature to support the 2nd and 3rd hypotheses of cold spot region formation (Figures 12, 13, and 14). During the initial dust storm month, there is an increase in non-topographic cold spot regions in the northern hemisphere Figure 15b. Knowing cold spot regions helped us to know the polar dynamics, CO_2 cycle, water cycle, and polar cloud regions.

As DDR data is not in the gridded format it is difficult to use direct DDR data for finding spatial and temporal variation. Need to incorporate radiance data from MCD RDR. These radiance data will help to correlate cold spots concerning grain size distribution of CO_2 and water ice. It will also provide data on surface soil features through emissivity data. There are fewer current works on cold spot regions. Need to apply an inclusive statistical model like The δ-Eddington approximation of the radiative transfer equation (RTE) that will better correlate polar clouds with cold spot formations (Hayne and Paige, 2008).

Other dust storm years' data could be used for comparative analysis in order to clarify the robustness of the results obtained. Also, using the radiance and statistical methods will provide more knowledge on the grain size distribution and polar clouds. Need to include a deep study on southern cold spot regions. Understanding cold spot regions means understanding the seasonal and dynamics-dependent carbon cycle and polar clouds on mars.

References

Hayne, P., & Paige, D. A. (2008, March). Mars Polar Cold Spots Observed by MRO Mars Climate Sounder. In 39th Annual Lunar and Planetary Science Conference (No. 1391, p. 2516). https://ui.adsabs.harvard.edu/abs/2008LPI....39.2516H/abstract

Cornwall, C., & Titus, T. N. (2009). Spatial and temporal distributions of Martian north polar cold spots before, during, and after the global dust storm of 2001. Journal of Geophysical Research: Planets, 114(E2). https://doi.org/10.1029/2008JE003243

Cornwall, C., & Titus, T. N. (2010). A comparison of Martian north and south polar cold spots and the long-term effects of the 2001 global dust storm. Journal of Geophysical Research: Planets, 115(E6). https://doi.org/10.1029/2009JE003514

Weiss, B. P., & Ingersoll, A. P. (2000). Cold spots in the Martian polar regions: evidence of carbon dioxide depletion?. Icarus, 144(2), 432-435. https://doi.org/10.1006/icar.1999.6302

Hayne, P. O., Paige, D. A., Schofield, J. T., Kass, D. M., Kleinböhl, A., Heavens, N. G., & McCleese, D. J. (2012). Carbon dioxide snow clouds on Mars: South polar winter observations by the Mars Climate Sounder. Journal of Geophysical Research: Planets, 117(E8). https://doi.org/10.1029/2011JE004040

Barrigar, D. B. (1963). A statistical investigation of the diurnal temperature variation during the polar night at McMurdo Sound, Antarctica (Doctoral dissertation, Monterey, California: US Naval Postgraduate School).

Määttänen, A., Vehkamäki, H., Lauri, A., Merikallio, S., Kauhanen, J., Savijärvi, H., & Kulmala, M. (2005). Nucleation studies in the Martian atmosphere. Journal of Geophysical Research: Planets, 110(E2). https://doi.org/10.1029/2004JE002308.

Montabone, L., Forget, F., Kass, D., Kleinboehl, A., Millour, E., Read, P., ... & Valeanu, A. (2019, September). Martian Year 34: A Case Study for the Onset, Evolution, and Impact of Large

Dust Storms on the Red Planet. In EPSC-DPS Joint Meeting 2019 (Vol. 2019, pp. EPSC-DPS2019). https://doi.org/10.1029/2004JE002308

Heavens, N. G., Kleinböhl, A., Chaffin, M. S., Halekas, J. S., Kass, D. M., Hayne, P. O., ... & Schofield, J. T. (2018). Hydrogen escape from Mars enhanced by deep convection in dust storms. Nature Astronomy, 2(2), 126-132.

Haberle, R. M., Pollack, J. B., Barnes, J. R., Zurek, R. W., Leovy, C. B., Murphy, J. R., ... & Schaeffer, J. (1993). Mars atmospheric dynamics as simulated by the NASA Ames General Circulation Model: 1. The zonal-mean circulation. Journal of Geophysical Research: Planets, 98(E2), 3093-3123. https://doi.org/10.1029/92JE02946

Clifford, S. M., Crisp, D., Fisher, D. A., Herkenhoff, K. E., Smrekar, S. E., Thomas, P. C., & Zwally, H. J. (2000). The state and future of Mars polar science and exploration. Icarus, 144(2), 210-242. https://doi.org/10.1006/icar.1999.6290

Ruff, S. W., & Christensen, P. R. (1999, July). Thermal-infrared spectral characteristics of Martian albedo features: Clues to composition. In The Fifth International Conference on Mars (p. 6230). https://ui.adsabs.harvard.edu/abs/1999ficm.conf.6230R/abstract